Chemistry–A European Journal

Full Paper
doi.org/10.1002/chem.202001703

Chirality

Coronenohelicenes with Dynamic Chirality

Corinna Weiss,[a] Dmitry I. Sharapa,[b] and Andreas Hirsch*[a]

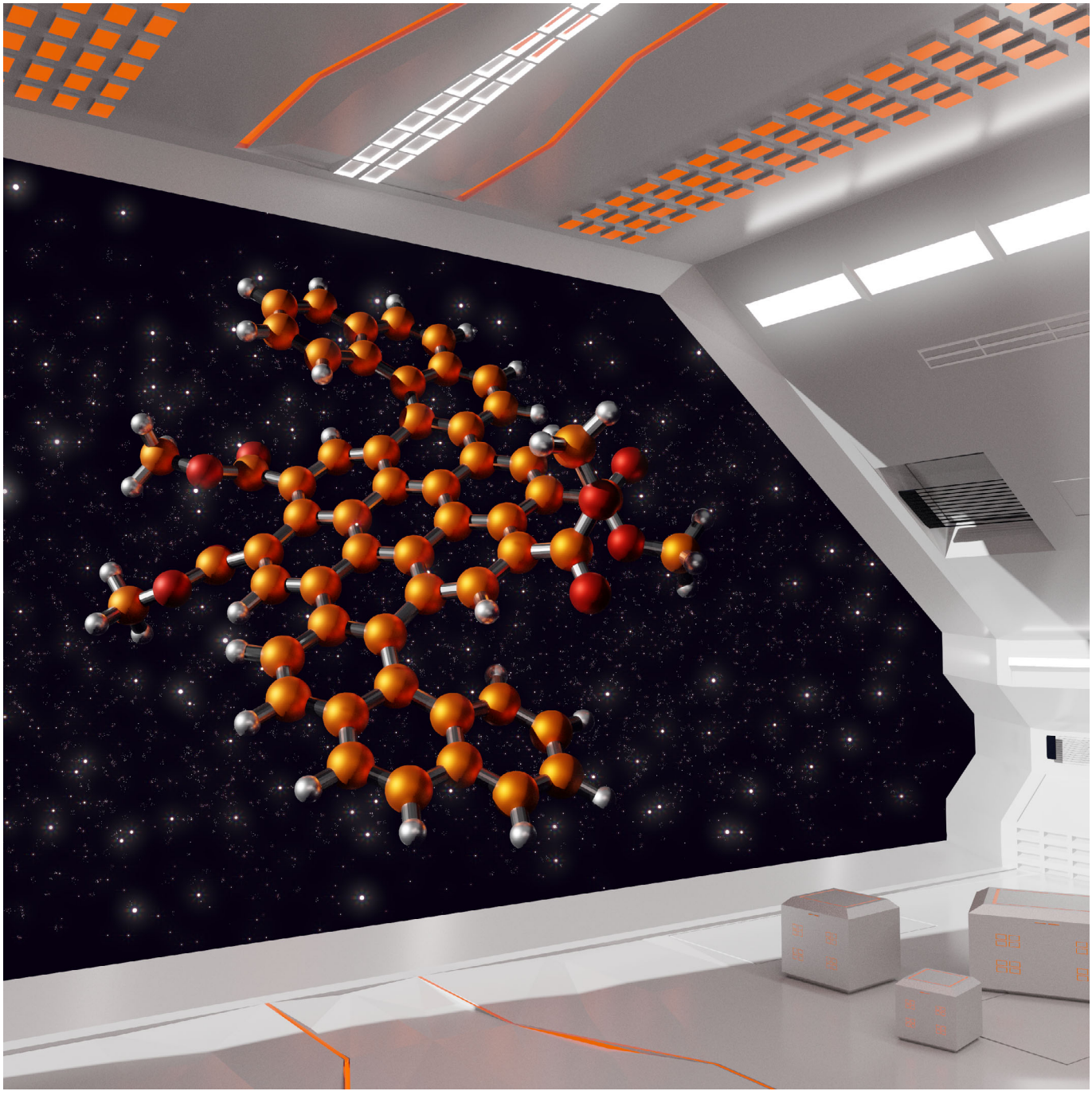

Abstract: The synthesis of a new type of chiral and dynamic nonplanar aromatics containing a combination of fused perylene-based coronenes and helicenes is reported. Either one or two helicene moieties were fused to the bay regions of an extended perylene core. The target compounds contain either identical or two different helicene building blocks. The combination with two helicene units leads to six different isomers, including two pairs of enantiomers and two *meso* forms. The experimental determination of the isomerization barriers the corresponding double [5]-helicenes revealed activation energies of $E_a = 24.81$ and 25.38 kcal mol^{-1}, which is slightly above the barrier of the parent [5]-helicene. Resolution of all possible regio- and stereoisomers allowed for the systematic investigation of the chiroptical properties. They revealed remarkable dissymmetry factors $|g_{abs}|$ of up to 1.2×10^{-2}, which mirror the synergy between the strong absorbing perylenes and the inherent chirality of helicenes.

Introduction

The field of nonplanar polyaromatic hydrocarbons (PAHs) is growing rapidly, not only due to their fascinating 3D-structures and hindered supramolecular aggregation leading to improved solubility and processability, but also due to their exceptional optical-, electronic-, dynamic- and other physical properties.[1] Among nonplanar PAHs helicenes stand out due to their pronounced chirality extending over the entire conjugated π-system. Helicenes have recently attracted increasing attention.[2] They consist of *ortho*-fused benzene rings which leads to a conformational distortion of their π system, resulting from steric repulsion.[3,4] Hence, chirality and chiroptical properties, such as strong circular dichroism is characteristic for helicenes.[3,4] They can adopt either a *P* (plus) or *M* (minus) configuration, depending on the sense of helicity. The different helicities can be interconverted into each other by overcoming an inversion barrier, which depends on the helicene size and the corresponding steric constraints.[5] These characteristics demonstrate their potential for applications in fields such as asymmetric catalysis, supramolecular chemistry, as chiroptical switches, spin filters and in nonlinear optics.[6] As a consequence further research in new structural types of helicenes continues to excite and remains challenging. In general, there are four different strategies tuning and improving the properties of helicenes: 1) Fusing a large number of *ortho*-connected benzene rings together to generate elongated helicenes. The longest helicene known so far is a [16]-helicene.[7] 2) Heterohelicenes, which are generated by incorporation of heteroatoms into the helicene framework.[5] 3) Combination of helicene motifs with other PAHs leading to pronounced Cotton effects due to the extension of the conjugated π-system.[5] In this respect especially the incorporation of large aromatics, such as hexa-*peri*-hexabenzocoronenes (HBCs)[1b,2a,8] or corannulenes has recently become an attractive task.[9] 4) Generation of multihelicenes, which contain two or more helicene units fused within one conjugated π-system. This latter helicene family is of great interest because a variety of confirmations can be adopted leading to structural diversity. Recently, first series of examples of multihelicenes, including two, five, six and even nine integrated helical motifs have been reported.[5,6,8e,h,i,9b,10] Moreover, a combination of lateral π-expansion with multihelicity within one molecule is an interesting target, as enhanced or even new properties might appear originating from the combination of both concepts. Apart from HBCs or corannulenes, perylene diimides are promising candidates for the mergence with helicenes since they provide various desirable properties themselves.[11] They feature intensely absorbing, chemically and thermally stable dyes and can easily be derivatized. Hence, they have potential to emerge as attractive building blocks, for example, in organic field effect transistors, organic photovoltaics, and supramolecular assemblies.[11] Some first prototypes of PDI-carbohelicene hybrids have already been reported (see Figure 1).[1a,10d,12]

These examples rely on the combination of one-to-six helicene motifs with several perylenes, thus generating sterically very congested structures with rather high inversion bar-

[a] C. Weiss, Prof. Dr. A. Hirsch
Department of Chemistry and Pharmacy
Friedrich-Alexander University Erlangen-Nürnberg
Nikolaus-Fiebiger-Straße 10, 91058 Erlangen (Germany)
E-mail: andreas.hirsch@fau.de

[b] Dr. D. I. Sharapa
Institute of Catalysis Research and Technology
Karlsruhe Institute of Technology
Hermann-von-Helmholtz-Platz 1, 76344 Eggenstein-Leopoldshafen (Germany)

Supporting information and the ORCID identification number(s) for the author(s) of this article can be found under: https://doi.org/10.1002/chem.202001703.

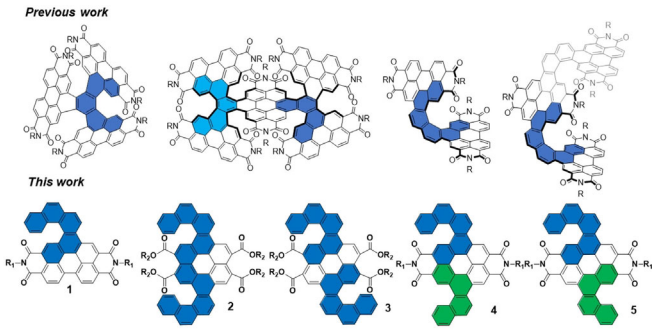

Figure 1. Previously reported perylene–helicene hybrids and new architectures **1**–**5** developed in this study.

riers.[1a,10d,12] In this contribution, however, we will report on an alternative approach merging one perylene core only with several helicenes. As a result, our compounds are sterically unresisted and dynamic which enables a study of their comparably low inversion barriers. The target molecules are symmetric **2**, **3** or asymmetric structures **4**, **5** which feature either two identical or two different [*n*]-helical moieties and show interesting dynamic behavior. Just recently, Liu et al. reported a similar approach combining a perylene with two [8]-helicenes resulting in structures with remarkable chiroptical properties.[13] However, their structures showed no isomerization at all due to the incorporation of larger helicene analogues. In this report, we describe the synthesis and characterization of new single and double helicene–perylene hybrids, resulting from the fusion of helicenes with either one or both bay regions of the perylenes. Mergence with naphthalene or phenanthrene units allows us to form the corresponding [4]-helicene and [5]-helicene derivatives. We separated the enantiomers and calculated the activation barriers for the helicity inversion process.

Results and Discussion

Synthesis and characterization

Scheme 1 illustrates the simple but versatile synthetic concept to prepare mono-helicene **1** as well as the symmetric bis-helicenes **2** and **3** and the asymmetric bis-helicenes **4** and **5**. Our strategy mainly included two key steps: 1) Suzuki couplings at the *bay* position of perylenes and 2) oxidative photocyclization of Suzuki products forming the corresponding closed helicene structures. Interestingly, we found that the photocyclization selectively stopped at the stage of [5]-helicenes and no additional bond formation towards a planar structure was observed. As starting materials for all helicenes mono- or dibrominated perylene diimides **6** or perylene tetraesters **7** were chosen. They are equipped with large aliphatic chains at the *peri* positions, which are necessary in order to provide sufficient solubility. As coupling partners naphthalene **9** as well as phenanthrene boronic ester **8** were used which needed to be functionalized in 1- and 4-position, respectively, in order to prevent unwanted side reactions. Phenanthrene boronic acid **8** was obtained by following a modified strategy starting from 1-naphthol as described by van der Meijden et al.[14]

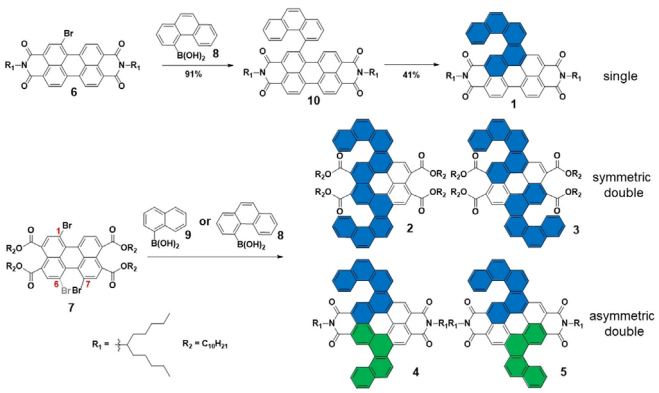

Scheme 1. Synthesis of compounds **1**–**5**.

Mono-[5]-helicene **1** was prepared starting directly from the monobrominated PDI **6** and subsequent Suzuki coupling and photocyclization afforded **1** as mixtures of *M* and *P* isomers. The structure assignment of **1** was accomplished by ^{1}H and ^{13}C NMR, HRMS, UV/Vis and fluorescence spectroscopy (Figure 2) measurements. Owing to the nonplanar helical structure **1** is very soluble in common organic solvents, such as dichloromethane, chloroform, ethyl acetate or toluene. It has an orange color in solution. Thus, the UV/Vis absorption spectrum of **1** shows several absorption bands in the visible region with a broad absorption at 313 nm and an extinction coefficient of 51 000 M^{-1} cm^{-1} and two smaller bands at 364 and 382 nm. At higher wavelengths three more bands were detected, showing a broad shoulder at approximately 430 nm and two distinct peaks at 480 and 514 nm, which show the typical perylene fine structure. When irradiated with UV light compound **1** reveals an intense orange fluorescence in solution with a remarkably small Stokes shift of 29 nm and a maximum at 543 nm. Interestingly, when comparing the absorption and emission of the opened **10** and closed **1** form, the spectra of **1** are hypsochromically shifted compared to **10**, which is caused by the increased aromaticity of **1**. The helical structure of **1** was confirmed by chiral HPLC using a Chiralpak 1BN-5 column. The two enantiomers with retention times $t_R = 8.8$ min and $t_R = 12.3$ min could be completely separated and were characterized with circular dichroism (CD) spectroscopy measurements. The mirror inverted spectra shown in Figure 2 display two high Cotton effects in the visible region between 250 to 300 nm and 350 to 400 nm with corresponding $|\Delta\varepsilon|$ of 90 $M^{-1}cm^{-1}$ and 43 $M^{-1}cm^{-1}$, respectively. Theoretical simulations based on sTD-DFT (for computational details see Supporting Information) are in agreement with the experimental data and assign the first eluted fraction as *M* and second eluted fraction as *P* isomer. The calculated dissymmetry factors $|g_{abs}|$ reach a maximum of 2.5×10^{-3} at 260 nm.

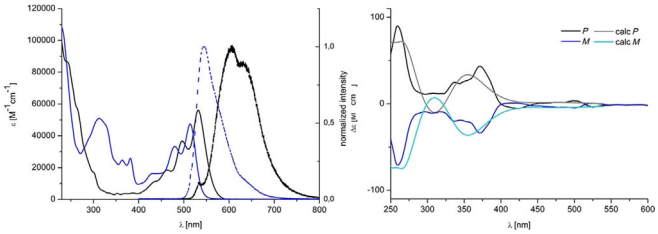

Figure 2. Left: UV/Vis absorption (solid line) and emission spectra (dotted line) of **1** (blue line) and **10** (black line). Right: measured (black, dark blue) and calculated (grey, light blue) CD spectra (sTD-wB97X-D3/def2-TZVP) of **1**.

When starting the synthesis from the dibrominated precursor **7** we obtained the bis-helicenes **2**, **3**, **4** and **5**, which contain one coronene core. Therefore, we can either obtain "symmetric" structures by coupling with two identical aromatic boronic acids or "asymmetric" structures by using two different boronic acids in two subsequent coupling reactions (see

Scheme 1). However, more sophisticated separation methods had to be applied in this case due to the formation of 1.6- and 1.7-functionalized isomers, which are already formed during bromination, as well as the *M* and *P* isomers. We found out that in our case it was easier to separate the brominated regioisomers after further functionalization rather than directly after bromination. In both cases, the symmetric as well as the asymmetric route, this functionalization included a Suzuki coupling with phenanthrene boronic acid **8** in the first step. When applying 2.5 equivalents of boronic acid we were able to obtain both the bis- and monoadducts as well as the different regioisomers in only one step. We succeeded in separating the twofold from the onefold Suzuki adducts through multiple plug filtrations and column chromatography as well as separating the 1.6- and 1.7-isomers by HPLC. For the monoadducts **11 a** and **11 b** we succeeded with the separation by a preparative Nucleosil column using recycling mode. The two isomers were both characterized by high resolution mass spectrometry and show very similar properties regarding UV/Vis and fluorescence spectroscopy. However, they could be distinguished by NMR spectroscopy (^{1}H, ^{13}C, COSY, HSQC/2D selective HSQC, HMBC/2D selective HMBC, DEPTq135, ROE, HOESY, see Supporting Information). Starting from the two monoadducts, 1.6-**11 a** and the 1.7-isomer **11 b**, the asymmetric structures **4** and **5** were synthesized, which contain a [4]-"helical" and a [5]-helical moiety. Another Suzuki coupling with naphthalene boronic acid **9** afforded the asymmetric structures **12** and **13**, resulting from the reactions with **11 a** and **11 b**, respectively (see Scheme 2).

We observed that the products were very sensitive to light and discovered that the 1.6-isomer **12** contained already some cyclized species **14** (see Supporting Information for synthetic details). Thus, **12** was directly irradiated to give **14** without further purification. However, we were able to isolate pure 1.7-isomer **13** which was subsequently irradiated to afford **15**. Lastly, the ester chains could be removed to recover the dianhydrides and thereafter introduce imides into the *peri* positions of **4** and **5**. This approach allows not only to tailor and switch the solubilities of helicenes but also to influence their optoelectronic behavior. Compounds **4** and **5** have very similar properties. Due to the nonplanar helical structure as well as the branched alkyl chains at imide positions they provide excellent solubility in various organic solvents, such as dichloromethane, chloroform and other chlorinated alkanes, toluene, polar solvents, such as ethyl acetate and tetrahydrofuran, and even sufficient solubility in nonpolar solvents, such as hexane or heptane. Compared to the tetraester precursors **14** and **15**, which are yellow-greenish, **4** and **5** have an intense orange color in solution and thus the UV/Vis spectra of **4** and **5** are bathochromically shifted compared to those of **14** and **15** (see Figure 3). For both, **4** and **5**, the longest wavelength absorption can be found at 541 nm. At lower wavelengths absorption bands were observed at around 500, 486 and 457 nm. The intense coronene bands were detected at 386 nm and 367 nm for both molecules with extinction coefficients of around 56 000 M^{-1} cm $^{-1}$. In the region between 250 and 330 nm **4** and **5** differ slightly, 1.6-isomer **4** absorbs at 313 and 276 nm while 1.7-isomer **5** shows only one strong absorption band at 282 nm. Regarding the molar extinction coefficients, the esters **14** and **15** show much higher values of up to 161 000 M^{-1} cm^{-1} compared to imides **4**, **5**. Moreover, in all cases, the 1.6-isomers absorb stronger and thus all 1.6-isomers have higher ε values than the corresponding 1.7-isomers. When irradiated with UV light ($\lambda = 366$ nm) esters **14** and **15** show an intense green fluorescence with emission bands at 496 and 530 nm, while the bands of **4** and **5** again are bathochromically shifted to 553 and 594 nm. Since **4** and **5** contain helicenes they are chiral molecules which could be separated by chiral HPLC and the enantiomers characterized with CD measurements. We found that the [4]-"helical" moiety of **4** and **5** isomerizes easily at room temperature and thus shows no chiral behavior while the barrier of the [5]-helical unit of **4** and **5** is sufficient large to observe the existence of *M* and *P* isomers (see Figure 3). In both cases theoretical studies assigned the first eluted fraction as *M* and the second eluted fraction as *P* isomer. The measured circular dichroism spectra of **4** and **5** differ significantly. While **4** exhibits only two main Cotton effects at wavelengths of around 280 and 380 nm with corresponding $|\Delta\varepsilon|$ of 88 and

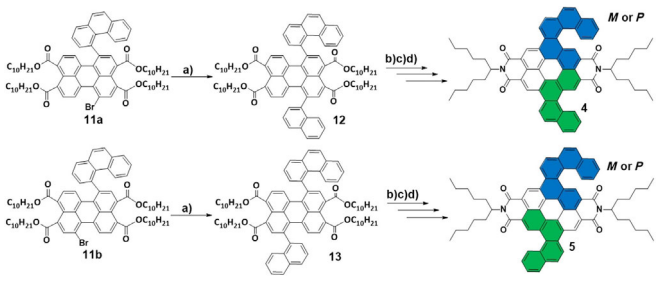

Scheme 2. Synthesis of **4** and **5**. Reaction conditions: (a) 2.5 equiv naphthalene boronic acid **9**, 7.6 equiv Na_2CO_3, 0.05 equiv $Pd(PPh_3)_4$, toluene/EtOH/H_2O, 80 °C, 17 h, 99% (**13**); (b) 0.05 equiv I_2, hν, toluene/THF, 8 h, 61% (**14**), 88% (**15**); (c) 3.0 equiv *p*TsOH, toluene/dodecane 1:5, 95 °C, 5 h; (d) 2.4 equiv 6-undecylamine, 160 °C, imidazole, 2 h, 58% (**4**), 80% (**5**).

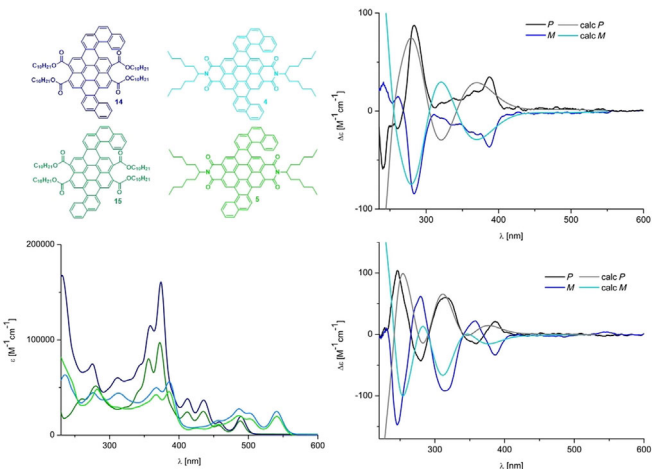

Figure 3. Left: UV/Vis absorption spectra of 1.6-tetraester **14** (dark blue), 1.6-diimide **4** (light blue), 1.7-tetraester **15** (dark green) and 1.7-diimide **5** (light green). Right: CD spectra of **4** (above) and **5** (below).

36 $M^{-1}cm^{-1}$, respectively, **5** shows an increased number of five Cotton effects at around 250, 275, 315, 360 and 390 nm as well as increased $|\Delta\varepsilon|$ values of up to 148 $M^{-1}cm^{-1}$ for 250 nm. The calculated $|g_{abs}|$ values reach up to 2.2×10^{-3} for **4** and 3.3×10^{-3} for **5**.

The symmetric structures **2** and **3** were synthesized by starting from the bifunctional Suzuki adducts **11c** and **11d** as depicted in Scheme 3. The isomers **11c** and **11d** were characterized by HRMS, they show similar UV/Vis and fluorescence properties (see Supporting Information) and only slightly shifted ^1H, ^{13}C NMR and HMBC spectra (see Supporting Information). However, they could be distinguished with DEPT*q* NMR spectroscopy, considering the different number of quaternary carbon atoms. While the 1,6-isomer **11c** has 14 chemically equivalent quaternary carbons, the quaternary carbons of the 1,7-isomer **11d** amount to 12. Finally, the eluted fractions were irradiated separately in order to selectively obtain compounds **2** and **3**. By cyclizing the major 1.7-isomer **11d** the coronenohelicenes **3** could be obtained and by reacting the minor 1.6-isomer **11c** the compounds **2** were obtained. The structures were both confirmed by APPI HRMS, showing mass peaks at 1336.7730 *m/z* (**2**) and 1336.7739 *m/z* (**3**), which is in excellent agreement with the calculated value of 1336.7726. Furthermore ^1H (see Figure 4), ^{13}C and EXSY NMR and UV/Vis and fluorescence spectroscopy was measured. Both compounds **2** and **3** absorb in the visible region, they show a yellow color in solution and have similar UV/Vis spectra (see Figure 4). The most prominent absorption features in both cases are the newly formed coronene bands at 358 (**3**), 360 (**2**) and 378 (**2**, **3**) nm. At higher wavelengths **2** and **3** show three main absorption bands at 415 (**3**), 416 (**2**), 439 (**2**, **3**) and the longest wavelength absorption at 488 (**2**,**3**) nm.

Interestingly, **3** showed an additional intense band at 286 nm which was not found in the spectrum of **2**. Despite of the similar position of the absorption bands, the molar extinction coefficients of **2** and **3** differ considerably and reach values of up to 90 000 $M^{-1}cm^{-1}$ for the 1.7-isomers **3**, which is more than three times higher compared to the value of 28 000 $M^{-1}cm^{-1}$ for the 1.6-isomer **2**. When irradiated with UV light, both coronenes show a bright-green fluorescence and thus the emission maxima were found at similar values of 498 and 532 nm for compound **2** and 496 and 530 nm for **3** (see Figure 4 A). Considering the ^1H NMR spectrum **2** and **3** (see Figure 4 B) show similar signals. The largest differences are found in the region between 4.00–4.60 ppm where the resonances of the OCH_2 units of the ester chains can be found. While the C_2-symmetric compound **3** shows four multiplets, each with an integral ratio of 2, **2** gives rise to less ordered signals in this region. Furthermore, all signals of **2** are slightly downfield-shifted compared to the signals of **3**. Conspicuously, the signals for the four coronene protons between 9.60 and 10.20 ppm split up into four singlets for both compounds. This phenomenon is a strong hint towards the existence of the two helical units. Caused by the introduction of two helicene moieties into one single molecule three helical isomers are formed during this last synthetic step. Independently of one another both helicene moieties can adopt either a *M* or a *P* configuration. This results in two enantiomers (**2a**/**b** and **3a**/**b**) with *MM* or *PP* configuration and one mesomer (**2c** and **3c**) with *MP* configuration. Since the *MP* mesomer is a diastereomer of *MM* and *PP* the two different configurations should be detectable by NMR spectroscopy.

Owing to similar R_f values of the different helical isomers, separation by multiple column chromatographic steps using dichloromethane/hexane mixtures as eluent and as well as HPLC separation was required. The diastereomers of **2** and **3** could be separated on a Nucleosil column, whereby two main species were isolated, the *MP* and the *MM* (or *PP*) diastereomer. Although [5]-helicenes are known to invert at room temperature[3] we found that our molecules **2** and **3** are stable enough to isolate the pure fractions as well as to carry out the spectroscopic characterization despite the short time frame where

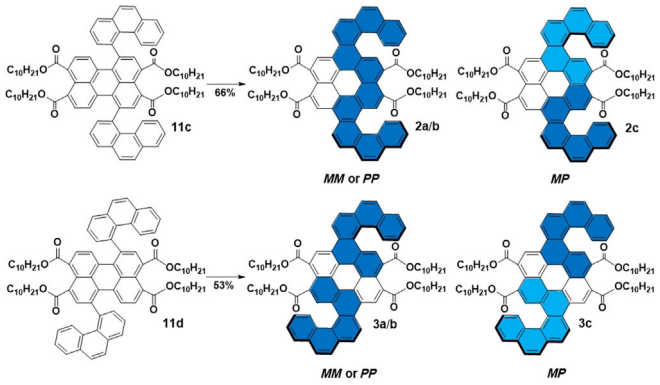

Scheme 3. Synthesis of compounds **2a**/**b**/**c** and **3a**/**b**/**c** with *M* helicenes in dark and *P* helicenes in light blue.

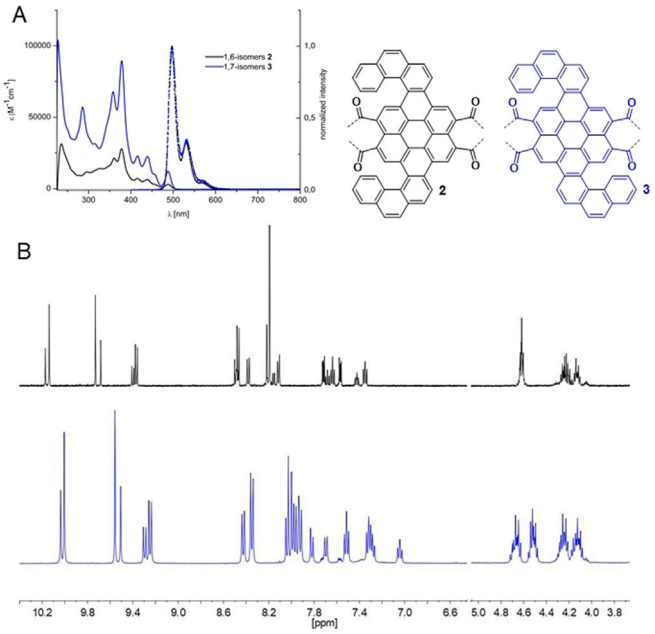

Figure 4. A) UV/Vis absorption and fluorescence spectra of **2** and **3**; B) partial ^1H NMR spectra of **2** (above) and **3** (below).

only one diastereomer was predominant (see Supporting Information). Fortunately, we further succeeded in displaying the switching of helicity by EXSY NMR spectroscopy (see Supporting Information). In order to assign the diastereomeric fractions as well as to investigate the properties of enantiomers we applied chiral HPLC. Considering the NMR data as well as the data obtained from chiral and nonchiral HPLC we found that in both cases the chiral species **2a/b** and **3a/b** with *PP* or *MM* configuration are more stable than the nonchiral **3c** and the *meso* forms **2c**. This is in stark contrast to the observations made by Liu *et al* who found a ratio of racemic and mesomeric types of 1:1.[13] The enantiomer separation of both, the 1.6 enantiomers **2a/b** and the 1.7-enantiomers **3a/b**, allowed us to investigate the CD properties shown in Figure 5. Theoretical studies were used to assign the helicity of separated fractions. All investigated compounds display Cotton effects in the region between 250 and 330 nm. However, the intensity differs significantly. While **2** reaches maximum $|\Delta\varepsilon|$ values of 152 $M^{-1}cm^{-1}$ for 244 nm, **3** shows remarkably high $|\Delta\varepsilon|$ values of up to 533 $M^{-1}cm^{-1}$ for 254 nm. Notably also the dissymmetric factors $|g_{abs}|$ observed for the 1.7-enantiomers **3a/b** reach exceptional high values of up to 1.2×10^{-2}, which is about one order of magnitude higher compared to the values of diimides **1**, **4** and **5** as well as compared to already reported derivatives.[8a, b, h, i]

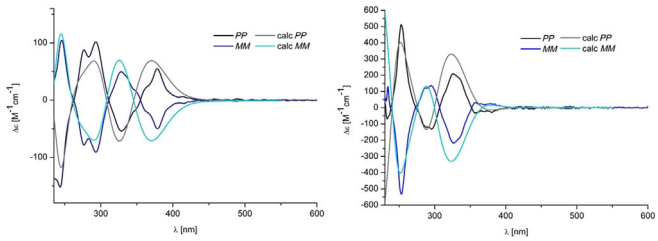

Figure 5. CD spectra of 1.6-enantiomers **2** (left) and 1.7-enantiomers **3** (right).

Isomerization studies

In order to estimate the stability and isomerization barrier of **2a/b** and **3a/b** we conducted further experiments. Since **2a/b** and **2c** as well as **3a/b** and **3c** are diastereomers, it was possible to follow the isomerization process between these with HPLC measurements (see Supporting Information for details) as well as by NMR spectroscopy (see Figure 6A). By using this approach isomerization barriers as well as the values for activation enthalpy and activation entropy can be estimated. In both cases, **2a/b** and **3a/b**, we chose to observe the inversion process from the more stable chiral isomers **2a/b** and **3a/b** to the less stable *meso* forms **2c** and **3c** (see Figure 6). For this purpose pure fractions **2a/b** and **3a/b**, obtained from HPLC separation, were investigated with a series of temperature dependent proton NMR measurements where the temperature was varied in 10 °C steps between 30 °C and 60 °C until an equilibrium between **2a/b** and **2c** (**3a/b** and **3c**) was reached. According to NMR data, 1.6-diastereomers **2a/b** and **2c** equilibrate at

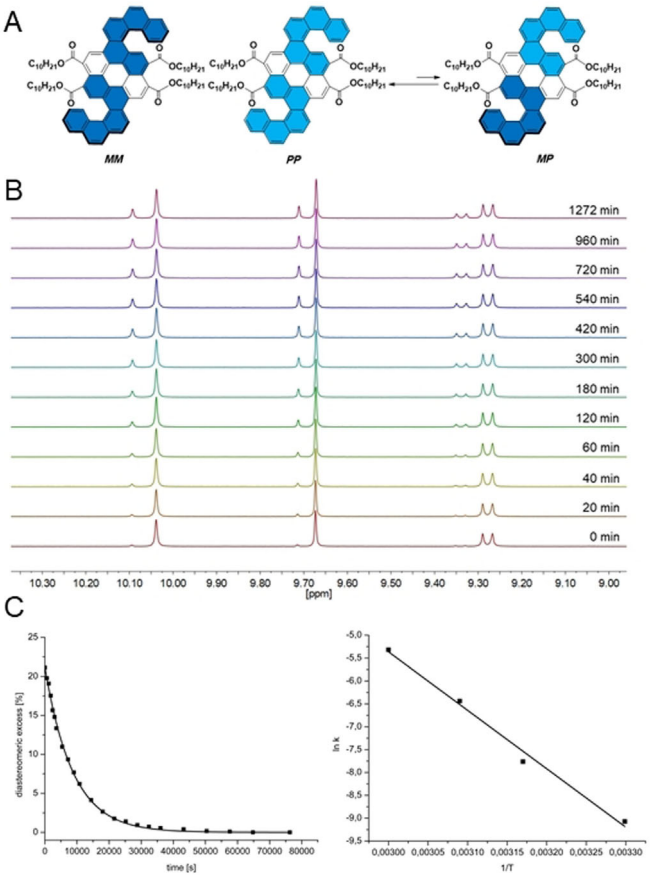

Figure 6. (A) Investigated isomerization process 1.7 **3a/b** **3c**. (B) ^{1}H NMR aromatic region of 1.7-isomers **3** at 30 °C over time. (C) Diastereomeric excess vs. time plot for decreasing concentration of 1.7-**3** at 30 °C (left) and Arrhenius plot (right).

a ratio of 1:2, while 1.7-diasteromers **3a/b** and **3c** level off at a ratio of 1:3. During a measurement series the change between pure diastereomer **2a/b** (**3a/b**) and diastereomeric mixture **2ab/2c** (**3ab/3c**) could be observed most unambiguously for the signals in the aromatic region between 7.10 and 10.15 ppm (see Figure 6A). Since the coronene singlets at around 9.70 and 10.10 ppm can be very reliably integrated due to excellent peak separation they were selected for the quantitative investigation of the isomerization process. All NMR measurements were analyzed by plotting the diastereomeric excess calculated from the integral ratio of the coronene singlets at around 9.70 ppm vs. the elapsed time. Considering Figure 6B, we can conclude that at 30 °C the equilibrium is reached after about 11 h. By fitting with an exponential fit $A = e^{-kT}$ rate constants were obtained. The obtained rate constants were then further used for an Arrhenius plot $\ln k$ vs. $1/T$ (see Figure 6C). From the slope $m = -E_a/R$ the activation barriers were calculated. We obtained similar values for both, the 1.6-isomers **2** with $E_a = 24.81$ kcal mol^{-1} and the 1.7-isomers **3** with $E_a = 25.38$ kcal mol^{-}. Both values are slightly higher than the literature known value of 23.50 kcal mol^{-} for the parent [5]-helicene.[3] This enlargement of the barrier of multiple helicenes compared to single helicenes is known in the literature and probably affected by π-extension and increased nonpla-

narity as well as structural interactions between the two helicenes.[4]

Additionally, when using the Eyring equation [Eq. (1)]

$$ln\frac{k}{T} = \frac{-\Delta H}{RT} + ln\frac{k_B}{h} + \frac{\Delta S}{R} \qquad (1)$$

and a plot of ln(k/T) vs. $1/T$ where k is the rate constant, T the measured temperature, R the gas constant, k_B the Boltzmann constant, h the Planck constant, ΔH the activation enthalpy and ΔS the activation entropy reaction parameters ΔH and ΔS can be obtained from the slope $m=-\Delta H/R$ and the y-intercept $\Delta S/R+\ln(k_B/h)$ (see Table 1). Additionally, we supported our observations with theoretical DFT calculations (see Figure 7, for computational details see Supporting Information). Helicity inversion proceeds through a two-step process involving two transition states, which both have the same energy but mirror image geometry. In both cases isomerization between *PP* and *MM* enantiomers starts with the conversion of *PP* into *meso MP* isomer by overcoming a first transition state *PP*/*MP* which is then converted into *MM* isomer by overcoming the second transition state.

The theoretical DFT-calculated stability of diastereomers **2** was opposite to the experimental observation of chiral forms **2a**/**b** being slightly more stable than *meso* form **2c**. The calculated energy values for **3** indicate a higher stability of **3a**/**b** compared to **3c** which is in agreement with experimental data. The calculated transition states have energy values of 29 kcal mol^{-1} for **2** and 25 kcal mol^{-1} for **3**, which are very similar to our experimentally determined values.

Table 1. Activation parameters of **2** and **3**.

Compounds	E_a [kcal mol^{-1}]	ΔH [kcal mol^{-1}]	ΔS [J mol^{-1} K^{-1}]
1.6-**2**	24.81	24.08	11.60
1.7-**3**	25.38	24.75	20.18

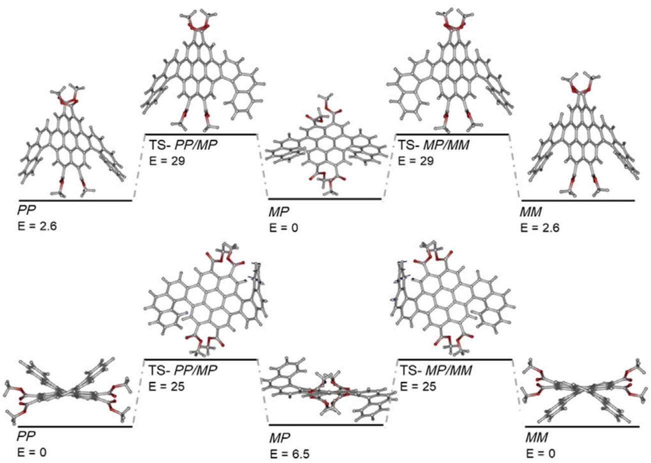

Figure 7. Energy diagram with calculated DFT energies (B3LYP, def2-SVP) for **2** (above) and **3** (below), energies given in kcal mol^{-1}.

Conclusions

In summary, we disclosed the access to a new family of mono- and bis-helicene–perylene hybrids. Our synthetic concept allows for the generation of both symmetric bis-helicenes involving two [5]-helicenes and asymmetric bis-helicenes involving one [4]-helical and one [5]-helical moiety. During the last photocyclization step of [5]-helicenes, no additional bond closure towards the planar structures was observed in any of the investigated cases. Photochemical studies indicated a significant blueshifted absorption for the closed helical structures compared to the opened perylene structures as well as a dependence on the solubilizing groups at the *peri* positions. Interestingly, the 1.6-and 1.7-regioisomers show in fact similar absorption bands but the molar extinction coefficients differ considerably. All enantiomers were separated by using chiral HPLC and their chiroptical behavior was investigated with CD measurements and supported by DFT calculations. The calculated dissymmetry factors $|g_{abs}|$ range from 2.1×10^{-3} up to 1.2×10^{-2} whereby the values for the perylene esters are significantly larger compared to the imides. Experimental determination of the helical inversion barriers of symmetric coronenohelicenes **2** and **3** revealed values of $E_a=24.81$ and 25.38 kcal mol^{-1}. Theoretical DFT studies supported our observations with values of $E_a=29$ kcal mol^{-1} and 25 kcal mol^{-1} for the inversion of **2** and **3**, respectively.

Experimental Section

Materials and instruments: Chemicals were purchased from Sigma–Aldrich and used without any further purification. Solvents were distilled prior to usage. Thin-layer chromatography (TLC) was performed on Merck silica gel 60 F524, detected by UV light (254 nm, 366 nm). Plug chromatography and column chromatography were performed on Macherey–Nagel silica gel 60 M (deactivated, 230–400 mesh, 0.04–0.063 mm). NMR spectra were recorded on a Bruker Avance 400 (^{1}H: 400 MHz, ^{13}C: 101 MHz), a Bruker Avance 500 (^{1}H: 500 MHz, ^{13}C: 126 MHz), or a Bruker Avance Neo Cryo-Probe DCH (^{1}H: 600 MHz, ^{13}C: 150 MHz). Deuterated solvents were purchased from Sigma–Aldrich and used as received. Chemical shifts are given in ppm at room temperature and are referenced to residual protic impurities in the solvents (^{1}H: $CHCl_3$: 7.24 ppm, CH_2Cl_2: 5.34 ppm, $C_2H_2Cl_4$: 5.91 ppm) or the deuterated solvent itself (^{13}C{^{1}H}: $CDCl_3$: 77.16 ppm, CD_2Cl_2: 53.4 ppm, $C_2D_2Cl_4$: 74.2 ppm). The resonance multiplicities are indicated as "s" (singlet), "brs" (broad singlet), "d" (doublet), "t" (triplet), "q" (quartet) and "m" (multiplet). Mass spectrometry was carried out with a Shimadzu AXIMA Confidence (MALDI-TOF, matrix: 2,5-dihydroxybenzoic acid DHB, *trans*-2-[3-(4-tert-butylphenyl)-2-methyl-2-propenyliden]-malononitrile, (DCTB) or without matrix (OM). High-resolution mass spectrometry (HRMS) was recorded on a LDI/MALDI-ToF Bruker Ultraflex Extreme machine or on a APPI-ToF mass spectrometer Bruker maXis 4G UHR MS/MS spectrometer. IR spectra were recorded on a Bruker FT- IR Tensor 27 spectrometer with a Pike MIRacle ATR unit. UV/vis spectroscopy was carried out on a Varian Cary 5000 UV-vis-NIR spectrometer. The spectra were recorded at rt in DCM in quartz cuvettes (edge length = 1 cm) under ambient conditions. Fluorescence spectra were obtained from a Shimadzu RF-5301 PC and a NanoLog spectrofluorometer (Horiba Scientific). Circular dichroism spectroscopy was measured at rt in DCM on a

Jasco J-815 spectrometer. HPLC separation was carried out using Shimadzu analytical and preparative HPLC with system controller CBM-20A, solvent delivery unit LC-20A, auto-sampler SIL-20A, column oven CTO-20A, photodiode array detector SPD-M202A, online degassing unit DGU-20A and low pressure gradient unit. All chromatograms were processed with Shimadzu LabSolution(c) software and exported as ASCII files.

General procedure A: Brominated perylene precursor and boronic acid were dissolved in toluene under nitrogen atmosphere and Na_2CO_3, EtOH and H_2O were added. After degassing $Pd(PPh_3)_4$ was added and the mixture was heated at 80 °C overnight. The reaction was cooled to rt, extracted with EtOAc and purified by filtration over silica gel.

General procedure B: Perylene precursors and iodine were dissolved in a toluene/THF mixture and irradiated until all educt was consumed. The solvent was evaporated and the crude mixture filtrated over silica gel.

General procedure C: Coronene tetraesters and *p*-toluenesulfonic acid were dissolved in a toluene and dodecane mixture and heated at 95 °C until all educt was consumed. Afterwards the reaction was cooled to rt, the solvent was evaporated and the crude mixture precipitated from CH_2Cl_2/MeOH. Afterwards water was added and the mixture was extracted with CH_2Cl_2.

General procedure D: Dianhydride precursors, 6-undecylamine and imidazole were heated at 140 °C for 2 h. Afterwards the reaction was cooled to rt, water was added and the mixture was extracted with CH_2Cl_2. The product was purified by plug filtration (SiO_2, CH_2Cl_2/hexane) and precipitated from dichloromethane/methanol.

Compound 1: The compound was prepared following general procedure B (**10:** 68.8 mg, 0.0787 mmol; iodine: 0.999 mg, 0.00394 mmol). Precipitation from CH_2Cl_2/MeOH yielded the product in 41% (28.0 mg, 0.0320 mmol). ^{1}H NMR (400 MHz, $C_2D_2Cl_4$, 373 K): δ = 10.18 (s, 1H), 9.69 (s, 1H), 9.25 (d, J = 8.4 Hz, 1H), 9.22 (d, J = 8.4 Hz, 1H), 9.14 (d, J = 8.6 Hz, 1H), 9.04 (d, J = 8.2 Hz, 1H), 8.98 (d, J = 8.2 Hz, 1H), 8.33 (d, J = 8.8 Hz, 1H), 8.24 (d, J = 8.4 Hz, 1H), 8.15 (d, J = 8.4 Hz, 1H), 8.09–8.06 (m, 2H), 7.59–7.54 (m, 1H), 7.23–7.14 (m, 3H), 5.34–5.26 (m, 1H), 5.17–5.10 (m, 1H), 2.39–2.29 (m, 2H). 2.27–2.19 (m, 2H), 2.04–1.94 (m, 2H), 1.88–1.78 (m, 2H), 1.44–1.28 (m, 24H), 0.87–0.82 ppm (m, 12H). ^{13}C NMR (101 MHz, $C_2D_2Cl_4$, 373 K): δ = 164.6, 135.1, 133.8, 133.3, 132.7, 131.1, 129.9, 129.7, 129.6, 129.5, 129.3, 128.7, 128.6, 127.9, 127.7, 127.42, 127.40, 127.1, 126.5, 125.9, 125.8, 124.57, 124.55, 124.0, 123.5, 123.1, 123.0, 122.9, 122.8, 122.1, 121.0, 55.3, 55.2, 54.9, 54.83, 54.80, 32.7, 31.8, 31.7, 31.6, 29.6, 26.7, 26.53, 26.49, 22.5, 22.4, 13.9 ppm. HRMS (MALDI-TOF, dctb): *m/z* for $C_{60}H_{62}N_2O_4$ calcd 872.4553, found 872.4545. UV/Vis: λ [nm] = 313 (ε = 50859 L mol^{-1} cm^{-1}), 364 (ε = 24699 L mol^{-1} cm^{-1}), 382 (ε = 25926 L mol^{-1} cm^{-1}), 480 (ε = 33365 L mol^{-1} cm^{-1}), 514 (ε = 47383 L mol^{-1} cm^{-1}). Fluorescence: λ [nm (λ_{ex} = 514 nm)] = 543.

Compound 4: : The compound was obtained following general procedure D (**16**: 4.51 mg, 0.00653 mmol; 6-undecylamine: 2.68 mg, 0.0157 mmol) whereby 58% (3.8 mg, 0.00381mmol) of red solid were obtained. ^{1}H NMR (400 MHz, $C_2D_2Cl_4$, 363 K): δ = 10.89 (s, 1H), 10.67 (d, J = 8.3 Hz, 2H), 10.28 (s, 1H), 9.53–9.33 (m, 3H), 8.46 (dd, J = 15.3, 8.8 Hz, 2H), 8.32 (dd, J = 7.8, 4.1 Hz, 2H), 8.22–8.09 (m, 3H), 8.07–8.00 (m, 1H), 7.93–7.85 (m, 1H), 7.63–7.57 (m, 1H), 7.20 (ddd, J = 8.3, 6.9, 1.2 Hz, 1H), 5.53–5.42 (m, 1H), 5.33–5.27 (m, 1H), 2.52–2.42 (m, 2H), 2.39–2.22 (m, 2H), 2.09 (m, 2H), 1.98–1.87 (m, 2H), 1.65–1.14 (m, 16H), 0.84 ppm (t, J = 7.2 Hz, 12H). ^{13}C NMR (151 MHz, $C_2D_2Cl_4$, rt): δ = 166.4, 165.9, 165.2, 165.1, 164.7, 134.1, 133.4, 133.0, 132.3, 131.8, 131.1, 131.0, 130.4, 130.3, 130.2, 130.0, 129.9, 129.7, 129.2, 129.02, 128.96, 128.6, 128.4, 128.3, 128.1, 128.01, 127.98, 127.8, 127.5, 127.0, 126.8, 126.7, 126.3, 125.9, 125.0, 124.3, 124.13, 124.06, 123.9, 123.8, 122.8, 122.7, 122.5, 122.1, 121.7, 121.3, 120.6, 120.1, 119.3, 117.1, 116.9, 116.7, 99.8, 80.1, 79.9, 79.7, 55.6, 55.2, 54.8, 32.9, 32.7, 32.6, 32.2, 32.2, 32.0, 31.9, 31.8, 30.03, 29.99, 29.7, 27.2, 27.0, 26.89 26.8, 23.2, 23.1, 23.0, 22.7, 14.6, 14.6, 14.5, 14.32, 14.27 ppm. HRMS (MALDI-TOF, dctb): *m/z* for $C_{70}H_{64}N_2O_4$ calcd 996.4866, found 996.4861. UV/Vis: λ [nm] = 276 (ε = 44665 L mol^{-1} cm^{-1}), 313 (ε = 44088 L mol^{-1} cm^{-1}), 367 (ε = 49779 L mol^{-1} cm^{-1}), 386 (ε = 56052 L mol^{-1} cm^{-1}), 457 (ε = 15367 L mol^{-1} cm^{-1}), 486 (ε = 27609 L mol^{-1} cm^{-1}), 501 (ε = 23036 L mol^{-1} cm^{-1}), 541 (ε = 24901 L mol^{-1} cm^{-1}). Fluorescence: λ [nm (λ_{ex} = 540 nm)] = 553, 594.

Compound 5: The compound was prepared following general procedure D (**17**: 22.5 mg, 0.0327 mmol; 6-undecylamine: 13.4 mg, 0.0785 mmol) whereby 80% (26.01 mg, 0.00262 mmol) of red solid were obtained. ^{1}H NMR (400 MHz, $C_2D_2Cl_4$, 363 K): δ = 10.93 (s, 1H), 10.60 (d, J = 11.5 Hz, 2H), 10.24 (s, 1H), 9.40 (dd, J = 9.0, 6.9 Hz, 3H), 8.47 (d, J = 8.9 Hz, 1H), 8.40 (d, J = 8.6 Hz, 1H), 8.31 (d, J = 8.1 Hz, 1H), 8.25 (d, J = 8.5 Hz, 1H), 8.16–7.99 (m, 4H), 7.89 (t, J = 7.5 Hz, 1H), 7.62–7.41 (m, 1H), 7.12 (ddd, J = 8.3, 6.9, 1.2 Hz, 1H), 5.52–5.40 (m, 1H), 5.35 -.24 (m, 1H), 2.53–2.42 (m, 2H), 2.36 (s, 2H), 2.16–2.04 (m, 2H), 1.99–1.87 (m, 2H), 1.60–1.17 (m, 24H), 0.85 ppm (t, J = 7.1 Hz, 9H). ^{13}C NMR (101 MHz, $C_2D_2Cl_4$, 363 K): δ = 165.4, 134.1, 133.3, 132.8, 132.5, 131.4, 131.0, 130.3, 130.2, 130.1, 129.6, 129.5, 129.4, 129.2, 128.9, 128.60, 128.55, 128.3, 128.1, 127.9, 127.74, 127.71, 127.6, 127.2, 127.0, 126.4, 126.0, 125.5, 124.7, 124.1, 124.1, 124.0, 123.9, 123.5, 122.5, 122.4, 122.3, 121.4, 55.5, 55.1, 32.9, 32.8, 32.4, 31.8, 31.74, 31.69, 29.6, 26.9, 26.8, 26.63, 26.60, 22.52, 22.45, 13.9 ppm. HRMS (MALDI-TOF, dctb): *m/z* for $C_{70}H_{64}N_2O_4$ calcd 996.4866, found 996.4868. UV/Vis: λ [nm] = 282 (ε = 48215 L mol^{-1} cm^{-1}), 367 (ε = 42490 L mol^{-1} cm^{-1}), 386 (ε = 45677 L mol^{-1} cm^{-1}), 425 (ε = 7349 L mol^{-1} cm^{-1}), 457 (ε = 11301 L mol^{-1} cm^{-1}), 486 (ε = 20527 L mol^{-1} cm^{-1}), 502 (ε = 17115 L mol^{-1} cm^{-1}), 541 (ε = 19699 L mol^{-1} cm^{-1}). Fluorescence: λ [nm (λ_{ex} = 541 nm)] = 553, 594.

Compound 2: The compound was prepared following general procedure B (**11 c**: 8.00 mg, 0.00597 mmol; iodine: 0.076 mg, 0.000299 mmol). The reaction progress was monitored by HPLC and afterwards the two coronene species were collected by preparative HPLC to yield 66% (5.31 mg, 0.00397 mmol) of the yellow product.^{1}H NMR (mixed isomers, 400 MHz, CD_2Cl_2, rt): δ = 10.10. 10.07 (2 s, 2H), 9.65, 9.63 (2 s, 2H), 9.37, 9.32 (2d, J = 9.1 Hz, 2H), 8.49, 8.42 (2d, J = 8.5 Hz, 4H), 8.19–8.03 (m, 6H), 7.62, 7.50 (2t, J = 7.4 Hz, 2H), 7.40–7.36, 7.25- 7.22 (2 m, 2H), 4.67–4.60 (m, 2H), 4.54–4.46 (m, 2H), 4.31–4.23 (m, 2H), 4.18–4.12 (m, 2H), 2.08–1.98 (m, 4H), 1.69–1.14 (m, 60H), 0.92–0.86 ppm (m, 12H). ^{1}H NMR (**2 a/b**, 400 MHz, $C_2D_2Cl_4$, 313 K): δ = 10.02 (s, 2H), 9.69 (s, 2H), 9.24 (d, J = 9.0 Hz, 2H), 8.34 (dd, J = 14.0, 8.6 Hz, 4H), 8.12–8.04 (m, 6H), 7.57 (t, J = 7.5 Hz, 2H), 7.31 (t, J = 8.2 Hz, 2H), 4.55–4.49 (m, 4H), 4.20–4.04 (m, 4H), 1.95–1.88 (m, 4H), 1.57–1.45 (m, 4H), 1.42–1.12 (m, 56H), 0.82-076 ppm (m, 12H). ^{1}H NMR (**2 c**, 400 MHz, $C_2D_2Cl_4$, 313 K): δ = 10.06 (s, 2H), 9.62 (s, 2H), 9.27 (d, J = 9.1 Hz, 2H), 8.40 (dd, J = 14.9, 8.6 Hz, 4H), 8.13–8.06 (m, 6H), 7.60 (t, J = 8.0 Hz, 2H), 7.38–7.34 m„ 2H), 4.53 (t, J = 6.9 Hz, 4H), 4.15–4.05 (m, 4H), 1.96–1.89 (m, 4H), 1.57–1.50 (m, 4H), 1.30–1.14 (m, 56H), 0.83–0.76 ppm (m, 12H). ^{13}C NMR (mixed isomers, 101 MHz, CD_2Cl_2, rt): δ [ppm] = 169.6, 169.3, 168.63, 168.56, 133.2, 132.9, 132.7, 132.5, 132.1, 131.7, 131.1, 130.9, 130.4, 130.1, 129,7, 129.35, 129.32, 129.2, 129.0, 128.82, 128.76, 128.6, 128.3, 127.9, 127.2, 127.0, 126.84, 126.78, 126.7, 126.6, 126.52, 126.49, 126.3, 126.2, 126.1, 126.0, 125.7, 125.42, 125.36, 125.2, 124.2, 123.9, 123.8, 123.5, 123.1, 123.0, 122.9, 122.2, 66.42, 66.39, 65.8, 63.2, 33.3, 32.4, 32.34, 32.30, 32.39, 30.14,

30.12, 30.10, 30.08, 30.05, 30.04, 30.02, 30.00, 29.98, 29.9, 29.84, 29.82, 29.80, 29.76, 29.74, 29.71, 29.20, 29.16, 28.8, 26.7, 26.1, 23.084, 23.077, 23.06, 14.262, 14.255, 14.25 ppm. HRMS (APPI): *m/z* for $C_{92}H_{110}O_8$ calcd 1336.7726, found 1336.7731. UV/Vis: λ [nm] = 360 (ε = 21 308 L mol^{-1} cm^{-1}), 378 (ε = 27 941 L mol^{-1} cm^{-1}), 416 (ε = 7184 L mol^{-1} cm^{-1}), 439 (ε = 6339 L mol^{-1} cm^{-1}), 488 (ε = 3059 L mol^{-1} cm^{-1}). Fluorescence: λ [nm (λ_{ex} = 488 nm)] = 498, 532.

Compound 3: The compound was prepared following general procedure B (**11 d**: 58.8 mg, 0.044 mmol; iodine: 0.560 mg, 0.00220 mmol). The reaction progress was monitored by HPLC and afterwards the two coronene species were collected via preparative HPLC to yield 53% (31.4 mg, 0.0234 mmol) of the yellow product. ^{1}H NMR (mixed isomers, 400 MHz, CD_2Cl_2, rt): δ = 10.10. 10.07 (2 s, 2H), 9.65, 9.63 (2 s, 2H), 9.37, 9.32 (2d, J = 9.1 Hz, 2H), 8.49, 8.42 (2d, J = 8.5 Hz, 4H), 8.19–8.03 (m, 6H), 7.62, 7.50 (2t, J = 7.4 Hz, 2H), 7.40–7.36, 7.25- 7.22 (2 m, 2H), 4.67–4.60 (m, 2H), 4.54–4.46 (m, 2H), 4.31–4.23 (m, 2H), 4.18–4.12 (m, 2H), 2.08–1.98 (m, 4H), 1.69–1.14 (m, 60H), 0.92–0.86 ppm (m, 12H). ^{1}H NMR (**3 a**/**b**, 400 MHz, $C_2D_2Cl_4$, 303 K): δ = 10.00 (s, 2H), 9.64 (s, 2H), 9.24 (d, J = 9.1 Hz, 2H), 8.39 (dd, J = 13.4, 8.8 Hz, 4H), 8.13–8.07 (m, 6H), 7.60 (t, J = 7.2 Hz, 2H), 7.39–7.29 (m, 2H), 4.53–4.47 (m, 2H), 4.42–4.37 (m, 2H), 4.22–4.16 (m, 2H), 4.11–4.06 (m, 2H), 1.93–1.88 (m, 4H), 1.55–1.50 (m, 4H), 1.44–1.07 (m, 56H), 0.84–0.76 ppm (m, 12H). ^{1}H NMR (**3 c**, 400 MHz, CD_2Cl_2, 313 K): δ = 10.11 (s, 2H), 9.64 (s, 2H), 9.36 (d, J = 9.1 Hz, 2H), 8.42 (d, J = 8.7 Hz, 2H), 8.20 (d, J = 8.5 Hz, 2H), 8.06 (d, J = 8.6 Hz, 2H), 8.00 (d, J = 8.5 Hz, 2H), 7.95 (d, J = 7.8 Hz, 2H), 7.54 (t, J = 7.1 Hz, 2H), 7.29–7.24 (m, 2H), 4.70–4.62 (m, 2H), 4.54–4.45 (m, 2H), 4.32–4.23 (m, 2H), 4.16 (dd, J = 10.7, 6.7 Hz, 2H), 2.39–2.28 (m, 4H), 2.10–2.00 (m, 6H), 1.72–1.16 (m, 54H), 0.92–0.80 ppm (m, 12H). ^{13}C NMR (mixed isomers, 101 MHz, CD_2Cl_2, rt): δ = 169.6, 169.3, 168.63, 168.56, 133.2, 132.9, 132.7, 132.5, 132.1, 131.7, 131.1, 130.9, 130.4, 130.1, 129,7, 129.35, 129.32, 129.2, 129.0, 128.82, 128.76, 128.6, 128.3, 127.9, 127.2, 127.0, 126.84, 126.78, 126.7, 126.6, 126.52, 126.49, 126.3, 126.2, 126.1, 126.0, 125.7, 125.42, 125.36, 125.2, 124.2, 123.9, 123.8, 123.5, 123.1, 123.0, 122.9, 122.2, 66.42, 66.39, 65.8, 63.2, 33.3, 32.4, 32.34, 32.30, 32.39, 30.14, 30.12, 30.10, 30.08, 30.05, 30.04, 30.02, 30.00, 29.98, 29.9, 29.84, 29.82, 29.80, 29.76, 29.74, 29.71, 29.20, 29.16, 28.8, 26.7, 26.1, 23.084, 23.077, 23.06, 14.262, 14.255, 14.25 ppm. HRMS (APPI): *m/z* for $C_{92}H_{110}O_8$ calcd 1336.7726, found 1336.7739. UV/Vis: λ [nm] = 286 (ε = 57 238 L mol^{-1} cm^{-1}), 358 (ε = 67 938 L mol^{-1} cm^{-1}), 378 (ε = 89 572 L mol^{-1} cm^{-1}), 415 (ε = 22 881 L mol^{-1} cm^{-1}), 439 (ε = 22 528 L mol^{-1} cm^{-1}), 488 (ε = 12 167 L mol^{-1} cm^{-1}). Fluorescence: λ [nm (λ_{ex} = 488 nm)] = 496, 530.

Acknowledgements

We thank the Deutsche Forschungsgemeinschaft (DFG), SFB 953 "Synthetic Carbon Allotropes" for financial support. Open access funding enabled and organized by Projekt DEAL.

Conflict of interest

The authors declare no conflict of interest.

Keywords: dynamic · helicene · isomerization · isomers · perylene

[1] a) N. J. Schuster, D. W. Paley, S. Jockusch, F. Ng, M. L. Steigerwald, C. Nuckolls, *Angew. Chem. Int. Ed.* **2016**, *55*, 13519 – 13523; *Angew. Chem.* **2016**, *128*, 13717 – 13721; b) T. Fujikawa, Y. Segawa, K. Itami, *J. Am. Chem. Soc.* **2015**, *137*, 7763.

[2] a) D. Reger, P. Haines, F. W. Heinemann, D. M. Guldi, N. Jux, *Angew. Chem. Int. Ed.* **2018**, *57*, 5938 – 5942; *Angew. Chem.* **2018**, *130*, 6044 – 6049; b) C. Zeng, C. Xiao, X. Feng, L. Zhang, W. Jiang, Z. Wang, *Angew. Chem. Int. Ed.* **2018**, *57*, 10933 – 10937; *Angew. Chem.* **2018**, *130*, 11099 – 11103.

[3] M. Gingras, G. Félix, R. Peresutti, *Chem. Soc. Rev.* **2013**, *42*, 1007 – 1050.

[4] K. Dhbaibi, L. Favereau, J. Crassous, *Chem. Rev.* **2019**, *119*, 8846 – 8953.

[5] K. Katao, Y. Segawa, K. Itami, *Synlett* **2019**, *30*, 370 – 377.

[6] a) T. Hosokawa, Y. Takahashi, T. Matsushima, S. Watanabe, S. Kikkawa, I. Azumaya, A. Tsurusaki, K. Kamikawa, *J. Am. Chem. Soc.* **2017**, *139*, 18512 – 18521; b) G. Liu, T. Koch, Y. Li, N. L. Doltsinis, Z. Wang, *Angew. Chem. Int. Ed.* **2019**, *58*, 178 – 183; *Angew. Chem.* **2019**, *131*, 184 – 189.

[7] K. Mori, T. Murase, M. Fujita, *Angew. Chem. Int. Ed.* **2015**, *54*, 6847 – 6851; *Angew. Chem.* **2015**, *127*, 6951 – 6955.

[8] a) C. M. Cruz, S. Castro-Fernández, E. Maçôas, J. M. Cuerva, A. G. Campaña, *Angew. Chem. Int. Ed.* **2018**, *57*, 14782 – 14786; *Angew. Chem.* **2018**, *130*, 14998 – 15002; b) C. M. Cruz, I. R. Márquez, S. Castro-Fernández, J. M. Cuerva, E. Maçôas, A. G. Campaña, *Angew. Chem. Int. Ed.* **2019**, *58*, 8068 – 8072; *Angew. Chem.* **2019**, *131*, 8152 – 8156; c) P. J. Evans, J. Ouyang, L. Favereau, J. Crassous, I. Fernández, J. Perles, N. Martín, *Angew. Chem. Int. Ed.* **2018**, *57*, 6774 – 6779; *Angew. Chem.* **2018**, *130*, 6890 – 6895; d) J. M. Fernández-García, P. J. Evans, S. Filippone, M. Á. Herranz, N. Martín, *Acc. Chem. Res.* **2019**, *52*, 1565 – 1574; e) T. Fujikawa, N. Mitoma, A. Wakamiya, A. Saeki, Y. Segawa, K. Itami, *Org. Biomol. Chem.* **2017**, *15*, 4697 – 4703; f) C. M. Cruz, S. Castro-Fernández, E. Maçôas, A. Millán, A. G. Campaña, *Synlett* **2019**, *30*, 997 – 1002; g) Y. Nakakuki, T. Hirose, H. Sotome, H. Miyasaka, K. Matsuda, *J. Am. Chem. Soc.* **2018**, *140*, 4317 – 4326; h) Y. Wang, Z. Yin, Y. Zhu, J. Gu, Y. Li, J. Wang, *Angew. Chem. Int. Ed.* **2019**, *58*, 587 – 591; *Angew. Chem.* **2019**, *131*, 597 – 601; i) Y. Zhu, X. Guo, Y. Li, J. Wang, *J. Am. Chem. Soc.* **2019**, *141*, 5511 – 5517.

[9] a) T. Fujikawa, D. V. Preda, Y. Segawa, K. Itami, L. T. Scott, *Org. Lett.* **2016**, *18*, 3992 – 3995; b) K. Kato, Y. Segawa, L. T. Scott, K. Itami, *Angew. Chem. Int. Ed.* **2018**, *57*, 1337 – 1341; *Angew. Chem.* **2018**, *130*, 1351 – 1355.

[10] a) Y. Hu, X.-Y. Wang, P.-X. Peng, X.-C. Wang, X.-Y. Cao, X. Feng, K. Müllen, A. Narita, *Angew. Chem.* **2017**, *129*, 3423 – 3427; b) H.-A. Lin, K. Kato, Y. Segawa, L. T. Scott, K. Itami, *Chem. Sci.* **2019**, *10*, 2326 – 2330; c) W.-B. Lin, M. Li, L. Fang, C.-F. Chen, *Chinese Chemical Letters* **2018**, *29*, 40 – 46; d) Q. Zhong, Y. Hu, K. Niu, H. Zhang, B. Yang, D. Ebeling, J. Tschakert, T. Cheng, A. Schirmeisen, A. Narita, K. Müllen, L. Chi, *J. Am. Chem. Soc.* **2019**, *141*, 7399 – 7406.

[11] a) J. Ma, L. Yin, G. Zou, Q. Zhang, *Eur. J. Org. Chem.* **2015**, 3296 – 3302; b) A. Nowak-Król, F. Würthner, *Org. Chem. Front.* **2019**, *6*, 1272 – 1318; c) P. Rajasingh, R. Cohen, E. Shirman, L. J. W. Shimon, B. Rybtchinski, *J. Org. Chem.* **2007**, *72*, 5973 – 5979; d) J. Vollbrecht, C. Wiebeler, A. Neuba, H. Bock, S. Schumacher, H. Kitzerow, *J. Phys. Chem. C* **2016**, *120*, 7839 – 7848; e) F. Würthner, *Chem. Commun.* **2004**, 1564 – 1579; f) Z. Yuan, Y. Xiao, Z. Li, X. Qian, *Org. Lett.* **2009**, *11*, 2808 – 2811; g) K. Nagarajan, A. R. Mallia, K. Muraleedharan, M. Hariharan, *Chem. Sci.* **2017**, *8*, 1776 – 1782; h) C. Lütke Eversloh, C. Li, K. Müllen, *Org. Lett.* **2011**, *13*, 4148 – 4150.

[12] a) N. J. Schuster, R. Hernández Sánchez, D. Bukharina, N. A. Kotov, N. Berova, F. Ng, M. L. Steigerwald, C. Nuckolls, *J. Am. Chem. Soc.* **2018**, *140*, 6235 – 6239; b) X. Liu, X. Du, J. Wang, C. Duan, X. Tang, T. Heumueller, G. Liu, Y. Li, Z. Wang, J. Wang, F. Liu, N. Li, C. J. Brabec, F. Huang, Y. Cao, *Adv. Energy Mater.* **2018**, *8*, 1801699.

[13] B. Liu, M. Böckmann, W. Jiang, N. L. Doltsinis, Z. Wang, *J. Am. Chem. Soc.* **2020**, *142*, 7092 – 7099.

[14] M. W. van der Meijden, T. Balandina, O. Ivasenko, S. de Feyter, K. Wurst, R. M. Kellogg, *Chemistry* **2016**, *22*, 14633 – 14639.

Manuscript received: April 8, 2020
Revised manuscript received: May 24, 2020
Accepted manuscript online: May 25, 2020
Version of record online: ■■ ▮▮, 0000

Full Paper
doi.org/10.1002/chem.202001703

FULL PAPER

Chirality

C. Weiss, D. I. Sharapa, A. Hirsch*

■■ – ■■

Coronenohelicenes with Dynamic Chirality

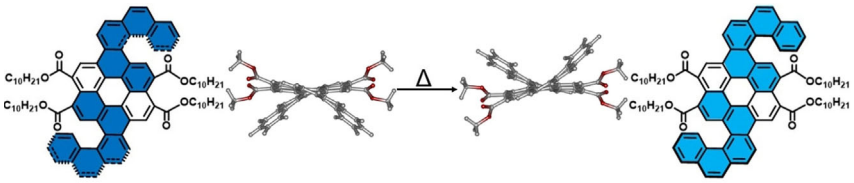

Dynamic helicenes: Double helicenes with a coronene core were synthesized. Temperature-dependent NMR experiments and DFT calculations shine light on the inversion process of the helicenes and revealed a two-step isomerization pathway. The isolated enantiomers exhibit remarkable optical and chiroptical properties.

Mono and double helicene–coronene hybrids were prepared by Pd-catalyzed cross-coupling and photocyclization reactions. The obtained helicenes are comparatively sterically unresisted and thus dynamic in solution which enabled a study of their inversion barriers. Temperature-dependent NMR experiments and DFT calculations shed light on the inversion process of the helicenes and revealed a two-step isomerization pathway. The isolated enantiomers exhibit remarkable optical and chiroptical properties. For more details see the Full Paper by A. Hirsch et al. on page ■■ ff.